Earthquakes and Structures, *Vol. 8, No. 1 (2015) 275-304*
DOI: http://dx.doi.org/10.12989/eas.2015.8.1.275

Dynamic response of a lined tunnel with transmitting boundaries

Mohammed Y. Fattah*, Mohammed J. Hamoo and Shatha H. Dawood

Building and Construction Eng. Dept., University of Technology, Baghdad, Iraq

(Received March 20, 2014, Revised August 9, 2014, Accepted August 20, 2014)

Abstract. The objective of this paper is to investigate the validity of transmitting boundaries in dynamic analysis of soil-structure interaction problems. As a case study, the proposed Baghdad metro line is considered. The information about the dimensions and the material properties of the concrete tunnel and surrounding soil were obtained from a previous study. A parametric study is carried out to investigate the effect of several parameters including the peak value of the horizontal component of earthquake displacement records and the frequency of the dynamic load. The computer program (Mod-MIXDYN) is used for the analysis. The numerical results are analyzed for three conditions; finite boundaries (traditional boundaries), infinite boundaries modelled by infinite elements (5-node mapped infinite element) presented by Selvadurai and Karpurapu 1988), and infinite boundaries modelled by dashpot elements (viscous boundaries). It was found that the transmitting boundary absorbs most of the incident energy. The distinct reflections observed for the "fixed boundaries" disappear by using "transmitted boundaries". This is true for both cases of using viscous boundaries or mapped infinite elements. The type and location of the dynamic load represent two controlling factors in deciding the importance of using infinite boundaries. It was found that the results present significant differences when earthquake is applied as a base motion or a pressure load is applied at the surface ground. The peak value of the vertical displacement at nodes A, B, E and F (located at the tunnel's crown and side walls, and at the surface above the tunnel and at the surface 6.5 m away from tunnel's centre respectively) increases with the frequency of the surface pressure load for both cases 1 and 2 (traditional boundaries and mapped infinite elements respectively) while it decreases for case 3 (viscous boundaries). The modular ratio Ec/Es (modulus of elasticity of the concrete lining to that of the surrounding soil) has a considerable effect on the peak value of the horizontal displacement at node B (on the side wall of the tunnel lining) increase about (17.5) times, for the three cases (1, 2, and 3).

Keywords: dynamic; soil-structure interaction; infinite element; tunnel; earthquake

1. Introduction

Many different approaches have been proposed for solving interaction problems considering infinite media by using a mechanism which irreversibly transfers energy from the near field to the far field. Generally, in analyzing the dynamic behavior of three dimensional structures, particularly when considering the soil-structure interaction or structure–soil-water interaction,

*Corresponding author, Professor, Ph.D., E-mail: myf_1968@yahoo.co
[a]Professor, E-mail: shatha1425@yahoo.com

http://www.techno-press.org/?journal=eas&subpage=7 ISSN: 2092-7614 (Print), 2092-7622 (Online)

modeling of continuous soil environment is necessary in order to illustrate the real behavior (Beer and Meek, 1981, Abdel-Fattah *et al*. 2000). Dynamic analysis of structures occurs in frequency domain or time domain. Where, analysis occurs in time domain by applying numerical methods, such as finite elements, it is necessary to mesh a limited length of the structure, form their equation of motion and after executing boundary conditions reach the results in the form of time history. In this kind of analysis, the effects of boundary conditions are effective in the attained results. Bettess (1977) and Zinkiewicz *et al*. (1983) have applied finite element method in such analysis.

Practically, in this analysis a combination of finite elements together with a few infinite or semi infinite elements have been utilized at the boundary points. Infinite elements shall be assumed in such a way that the material used shall continue indefinitely and their deformation shall become zero at infinity (real situation).

The viscous boundaries have been widely used for various wave propagation problems. But the number of finite elements required can still be large, as such boundaries are usually capable of transmitting plane or cylindrical waves only, and therefore they must be placed far from the initially disturbed region. FE cloning method for nonlinear dynamic problems involves the inverse of Fast Fourier Transform to obtain the time domain results. The boundary element method does not require domain discretization and allows a reduction in the spatial dimensionality, but the matrix is non-symmetric, non-positive definite and fully populated for single domains and block banded for multi-domains.

Infinite element can be regarded as the natural extension of the finite element to treat unbounded domain. In the infinite element method, the near field is modeled by finite elements and the far field is modeled by infinite elements. From the algorithmic point of view, the infinite element is treated as a standard finite element exceptfor the infinite approximation in the infinite direction. So the accuracy of the numerical solution depends only on the finite element method. The development of the infinite element has been receiving increased attention. The infinite element is very successful in elastostatics, consolidation analysis, seepage flow, hydrodynamics, acoustics and other fields. Medina and Penzien (1982), Medina and Taylor (1983), However, there were limitations to deal with structures having complex geometries and to solve the multiple wave components in layered soil media. Yun *et al*. (1995) developed more effective infinite elements for layered media. Zhao and Valliappan (1993) proposed and developed three dimensional (3D) infinite elements of mapped type, respectively. However, only frequency domain elements have been developed for solving dynamic problems. Recently, the elastodynamic infinite elements have been developed by using wave functions containing various wave components. One of the major drawbacks of the method is the necessity of a fundamental solution to exist. Such an analytical solution is difficult to derive.

An efficient stiffness design method for building structures was proposed by Takewaki *et al*. (2002) in which nonlinear soil amplification and soil–structure interaction were taken into account in terms of equivalent linearization. A sway-rocking shear building model with appropriate ground impedances derived from both finite-element analysis and the equivalent linearization technique was used as a simplified design model and super-structure stiffnesses satisfying a desired stiffness performance condition were determined for a ground-surface response spectrum. The ground-surface response spectrum was transformed from the design response spectrum defined at the upper surface level of the engineering bedrock via the equivalent linearization technique and the one-dimensional wave propagation theory. In the process of the super-structure stiffness design, an improved and advanced inverse formulation was developed which regards the fundamental natural

frequency of the interaction model as a principal design parameter. The reliability and accuracy of the proposed stiffness design method were examined by a two-dimensional finite-element model. Inelastic response characteristics of the so-designed model were also investigated.

Assortment of boundary conditions has an effect on dynamic responses. To reduce such effects, usually the length of the track is chosen to such a measure to minimize the dynamic responses of the end points of the track elements to zero. Doing so would cause an increase in the length of the track and hence add to an equation's degrees of freedom, volume of output and prolongation of analysis time. For this reason, a combination of finite elements and infinite beam elements (two end elements) was proposed by Zakeri and Xia (2009) for railway track modeling. Also, matrices of mass, damping and stiffness of one infinite element which has been laid on a visco-elastic bed, have been calculated by implementing selected shape functions. Therefore, by applying two infinite beam elements on either side of the model, a railway track is formed like a beam on an elastic bed which creates the possibility of eliminating the boundary condition effects.

The work of Ryu *et al*. (2010) proposed slightly new three-dimensional radial-shaped dynamic infinite elements fully coupled to finite elements for an analysis of soil–structure interaction system in a horizontally layered medium. The analysis dealt with a seismic analysis technique for a three-dimensional soil–structure interactive system, based on the coupled finite–infinite method in frequency domain. The dynamic infinite elements are simulated for the unbounded domain with wave functions propagating multi-generated wave components. The accuracy of the dynamic infinite element and effectiveness of the seismic analysis technique may be demonstrated through a typical compliance analysis of square surface footing, an L-shaped mat concrete footing on layered soil medium and two kinds of practical seismic analysis tests. The practical analyses are (1) a site response analysis of the well-known Hualien site excited by all travelling wave components (primary, shear, Rayleigh waves) and (2) a generation of a floor response spectrum of a nuclear power plant. The obtained dynamic results show good agreement compared with the measured response data and numerical values of other soil–structure interaction analysis package.

Birk and Behnke (2010) carried out dynamic analysis of arbitrarily shaped three dimensional foundations on layered ground using a coupled FEM-SBFEM approach. A novel scaled boundary finite element method for the analysis of three-dimensional layered continua over rigid bedrock is derived. The accuracy of the new method is demonstrated using rigid circular foundations resting on or embedded in nonhomogeneous soil layers as examples. The proposed modified formulation significantly broadens the area of application of the scaled boundary finite element method. It can be used for the frequency-domain analysis of 3D elastic foundations of arbitrary shape embedded in or resting on layered inhomogeneous soil. Its extension to the time-domain is the subject of current research.

Patil *et al*. (2010) presented an improved solution algorithm based on finite element method for the dynamic analysis of rigid pavements resting on Pasternak's two parameter soil medium. The concrete pavement is discretized by finite and infinite plate elements. Infinite elements are helpful in appropriate modelling of end conditions. In the underlying Pasternak soil medium the soft subgrade soil is modeled by spring elements and the base course is modeled by Pasternak shear layer. A parametric study is conducted to investigate the effect of various soil and pavement parameters on the response of pavement.

The effect of soil-structure interaction on the dynamic response of structures has been examined by Mahmoudpour *et al*. (2011). The substructure method using dynamic stiffness of soil was used to analyze soil-structure system. A coupled model based on finite element method and

scaled boundary finite element method is applied. Finite element method was used to analyze the structure, and scaled boundary finite element method is applied in the analysis of unbounded soil region. Due to analytical solution in the radial direction, the radiation condition is satisfied exactly. The material behavior of soil and structure was assumed to be linear. The soil region is considered as a homogeneous half-space. The analysis was performed in time domain. A computer program was prepared to analyze the soil-structure system. Comparing the results with those in literature shows the exactness and competency of the proposed method.

Equivalent dynamic infinite element was proposed by Su and Wang (2013). The idea of the method was based on the elastic recovery of general infinite element and the energy absorption of viscous boundary. The equivalent dynamic infinite element was not required for wave functions, since the waves on the interfaces with adjacent finite and infinite elements are absorbed by the equivalent damping. And the role of the far field medium in the elastic recovery has also been considered in the equivalent dynamic element. Such an element can be used directly as general finite element and appropriates for dynamic soil–structure interaction problems. Numerical analyses involving comparisons with known analytical or numerical solutions are presented. The results obtained show the effectiveness of the proposed equivalent dynamic infinite element.

The purpose of this research is to investigate the validity of using transmitting boundaries in dynamic analysis of soil-structure interaction problems. As a case study the proposed Baghdad metro line will be considered. A parametric study is carried out to investigate the effect of several parameters. These parameters are: the peak value of the horizontal component of earthquake displacement records, the tunnel diameter and the modular ratio of the concrete lining and the surrounding soil.

2. Local and non local absorbing boundaries

Absorbing boundary conditions can be subdivided in two main classes: local and non-local absorbing boundaries. When the absorbing boundary condition is local in space, the direct coupling of the degrees of freedoms is limited to one element of the boundary. In contrast, a non local (in space) absorbing boundary condition directly couples all degrees of freedom of the entire boundary (Feltrin 1997).

Generally, non-local absorbing boundary conditions are used in the context of frequency-domain analysis because the Fourier transform cancels the non-localness with respect to time. But in frequency domain analysis, the near as well as the far field have to behave linearly. In contrast, local absorbing boundary conditions are used in the context of time domain analysis. Hence they can be applied in nonlinear finite element analysis (near field nonlinear, far field linear) as well. However, because the accurate absorbing boundary conditions of wave dynamics are non-local in space and in time, local absorbing boundary conditions are necessarily approximations.

Examples of non-local absorbing boundaries in the frequency domain are the boundary integral method, the boundary element method, coupled finite element/boundary element method and some types of infinite elements in wave dynamics. Non local absorbing boundaries in the time domain (the convolution integral approach) are usually derived from the associated frequency domain by way of the inverse Fourier transform. Examples of local absorbing boundaries in the time domain are the viscous boundaries developed by Lysmer and Kuhlemeyer (1969) and the absorbing boundaries proposed by Engquist and Majda (1979).

3. Infinite elements

It is convenient to classify infinite elements as of static or dynamic type, as the methods needed for the two types are quite different. For static infinite elements, mapped and decay function type can also be used for some dynamic problems.

- **Static Infinite Elements**

The succeeding infinite element formulations have followed two main lines of development (Bettess, 1992):

a. Mapping of the element from finite to infinite domain.
b. Using decay functions in conjunction with the ordinary finite element shape function.

- **Mapped Infinite Elements**

Most of the proposed infinite elements adopted the idea of mapping, or can be cast in that form. In 1977, Ungless and Anderson used a term of form $1/(1+r)$ (r is the radial direction) in three dimensional elasticity applications. Medina and Penzin (1982) adopted the same approach. The first explicit stated mapping was made by Beer and Meek (1981), who used a mapping which included the terms ξ_0 :

$$2\,(\xi_j+\tfrac{1}{2})\,\xi \qquad \text{for } \xi < 0 \tag{5}$$

$$2\,(\xi_j+\tfrac{1}{2})\,\xi/(1-\xi) \qquad \text{for } \xi > 0 \tag{6}$$

They split the mapping into two parts, that from $\xi = -1$ to $\xi = 0$ and from $\xi = 0$ to $\xi = 1$. The procedure used was fairly complicated.

4. Selvadurai and karpurapu mapped infinite elements

In 1986, Selvadurai and Karpurapu have extended the scope of mapped type infinite elements to analyze the response of two-phase media such as saturated soils. The technique based on conventional shape functions and Gauss-Legendre numerical integration was used, thus making these elements suitable for implementation in general purpose finite element programs. This kind

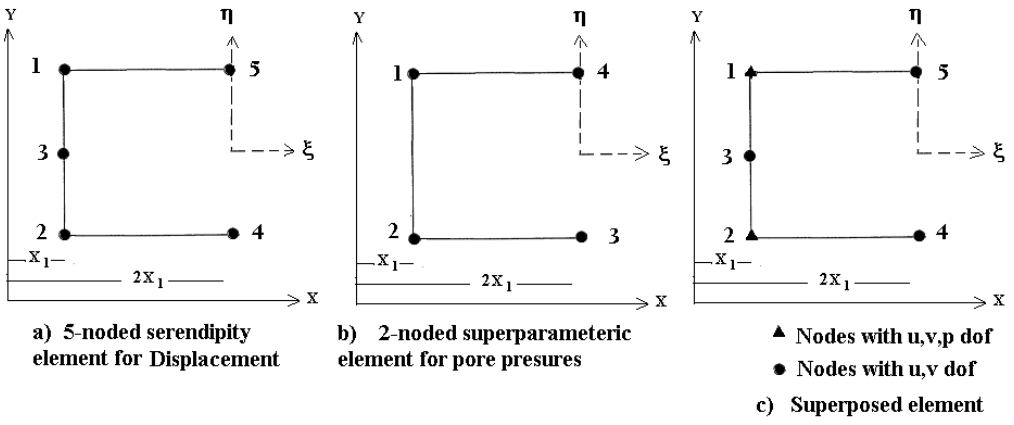

Fig. 1 Composite infinite elements in ξ direction (Karpurapu 1988)

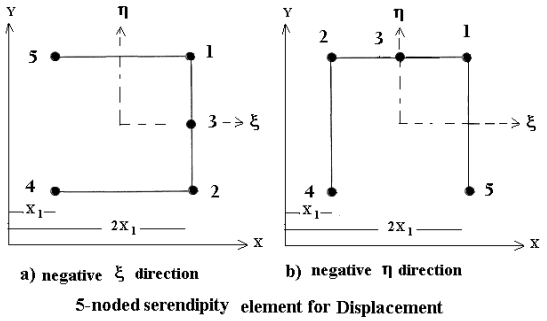

Fig. 2 The composite infinite elements adopted in this study for cases (a) and (b)

of elements was successfully employed for modeling many geomechanics problems (Karpurapu, 1988). Fig. 1 illustrates the composite infinite elements extended to infinity in ξ direction and Ttable 1 reports their mapping functions, derivatives and shape functions.

In this study, the derivation of the mapping functions for the infinite elements will be carried out for two different cases:

case (a) : Infinite element extended to infinity in the negative ξ direction.

case (b) : Infinite element extended to infinity in the negative ξ direction.

Fig. 2 presents the composite infinite element, while Tables 2 and 3 report the mapping functions and the derivatives for cases a and b.

5. Computer program

The computer program called "MIXDYN" (Owen and Hinton, 1980) was modified to (Mod-MIXDYN) by implementing the mapped infinite elements to it; i.e., 5-noded coding of the mapped infinite element extended from that presented by Selvadurai and Karpurapu in 1988. The program Mod-MIXDYN is coded in Fortran language and implemented on a Pentium-IV personal computer.

In this paper, the 5-nodeed serendipity mapped infinite element has also been added to the finite element models of the computer program (Mod-MIXDYN).

6. Description of the case study

The proposed Baghdad metro line consists of two routes of 32 km long and 36 stations designed as fortified shelters, as a first stage. The tunnel of reinforced concrete has a circular cross section with 5.0 m inner diameter (Diam.) and a 0.45 m lining thickness. The reinforcement details and the method of construction were not known. A typical geological section for a specified position which is characterized by a tunnel axis depth of 18 m is shown in Fig. 3. This figure also illustrates the soil properties of the three layers that characterize the investigated section. The properties of the materials involved in the problems are detailed in Table 5.

Table 1 Mapping and shape functions for composite mapped infinite element (Karpurapu 1988).
a. Mapping functions and derivatives

Node, i	2-noded Superparametric Mi	5-noded Serendipity isoparametric Mi	5-noded $\partial Mi/\partial\xi$	5-noded $\partial Mi/\partial\xi$
1	$-\xi(1+\eta)/\ (1-\xi)$	$-\xi\eta(1+\eta)/\ (1-\xi)$	$-\eta(1+\eta)/\ (1-\xi)^2$	$-\xi\,(1+2\eta)/(1-\xi)$
2	$-\xi(1-\eta)/\ (1-\xi)$	$\xi\eta(1-\eta)/\ (1-\xi)$	$\eta(1-\eta)/\ (1-\xi)^2$	$\xi(1-2\eta)/(1-\xi)$
3	$(1+\xi)(1-\eta)\ /2(1-\xi)$	$-2\xi(1-\eta^2)/\ (1-\xi)$	$-2(1-\eta^2)/\ (1-\xi)^2$	$4\xi\eta/(1-\xi)$
4	$(1+\xi)(1+\eta)\ /2(1-\xi)$	$(1+\xi)(1-\eta)\ /2(1-\xi)$	$(1-\eta)\ /(1-\xi)^2$	$-(1+\xi)/2(1-\xi)$
5		$(1+\xi)(1+\eta)\ /2(1-\xi)$	$(1+\eta)\ /(1-\xi)^2$	$(1+\xi)/2(1-\xi)$

b. Shape Functions

Node, i	2-noded Superparametric Ni	5-noded Serendipity isoparametric Ni
1	$(1-\xi)(1+\eta)/4$	$(1-\xi)(1+\eta)/4-(1-\xi^2)(1+\eta)/4-(1-\xi)(1-\eta^2)/4$
2	$(1-\xi)(1-\eta)/4$	$(1-\xi)(1-\eta)/4-(1-\xi)(1-\eta^2)/4-(1-\xi^2)(1-\eta)/4$
3		$(1-\xi)(1-\eta^2)/2$
4		$(1-\xi^2)(1-\eta)/2$
5		$(1-\xi^2)(1+\eta)/2$

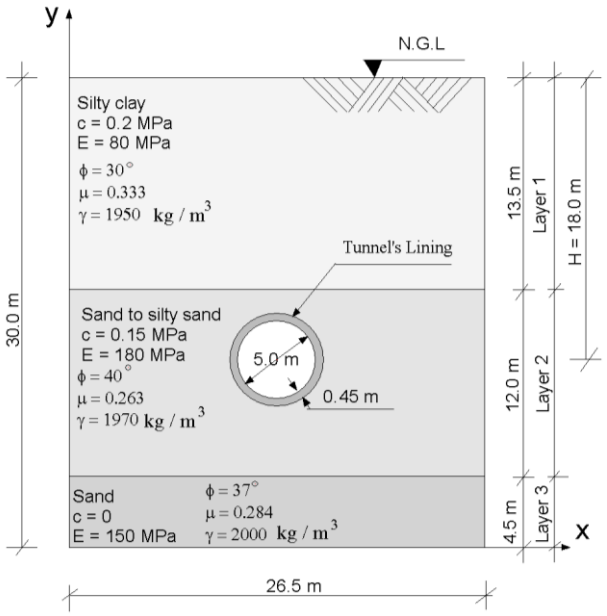

Fig. 3 Geological profile of the investigated Baghdad metro line section

Table 2 Mapping functions and their derivatives of the 5-noded serendipity mapped infinite element adopted in this study for case (a)

Node, i	ξ_i	ξ_i	5-noded serendipity Mi case a.	5-noded $\partial Mi/\partial\xi$	5-noded $\partial Mi/\partial\xi$
1	1	1	$\xi\eta(1+\eta)/\ (1+\xi)$	$\eta(1+\eta)/\ (1+\xi)^2$	$\xi(1+2\eta)/(1+\xi)$
2	1	-1	$-\xi\eta(1-\eta)/\ (1+\xi)$	$-\eta(1-\eta)/\ (1+\xi)^2$	$-\xi(1-2\eta)/(1+\xi)$
3	1	0	$2\xi(1-\eta^2)/\ (1+\xi)$	$2(1-\eta^2)/\ (1+\xi)^2$	$-4\xi\eta/(1+\xi)$
4	-1	-1	$(1-\xi)(1-\eta)\ /2(1+\xi)$	$(-1+\eta)\ /(1+\xi)^2$	$-(1-\xi)/2(1+\xi)$
5	-1	1	$(1-\xi)(1+\eta)\ /2(1+\xi)$	$-(1+\eta)\ /(1+\xi)^2$	$(1-\xi)/2(1+\xi)$

Table 3 Mapping functions and their derivatives of the 5-noded serendipity mapped infinite elements adopted in this study for case (b)

Node, i	ξ_i	ξ_i	5-noded serendipity Mi case b	5-noded $\partial Mi/\partial\xi$	5-noded $\partial Mi/\partial\xi$
1	1	1	$\xi\eta(1+\xi)/\ (1+\eta)$	$\xi(1+\xi)/\ (1+\eta)^2$	$\eta(1+2\xi)/(1+\eta)$
2	-1	1	$-\xi\eta(1-\xi)/\ (1+\eta)$	$-\xi(1-\xi)/\ (1+\eta)^2$	$-\eta(1-2\xi)/(1+\eta)$
3	0	1	$2\eta(1-\xi^2)/\ (1+\eta)$	$2(1-\xi^2)/\ (1+\eta)^2$	$-4\xi\eta/(1+\eta)$
4	-1	-1	$(1-\xi)(1-\eta)\ /2(1+\eta)$	$(-1+\xi)/\ (1+\eta)^2$	$-(1-\eta)/2(1-\eta)$
5	1	-1	$(1+\xi)(1-\eta)\ /2(1+\eta)$	$(-1-\xi)/\ (1+\eta)^2$	$(1-\eta)/2(1-\eta)$

Table 4 General information about the mesh adopted for the three different cases

Type of information		Case (1) Finite elements only	Case (2) Finite and infinite elements	Case (3) Finite and dashpot elements
No. of nodes		544	581	618
No. of finite elements		160	160	160
No. of infinite elements		-	20	-
No. of dashpot elements		-	-	50
No. of restrained nodes		37	37	50
Analysis type		Plane strain, Large displacement		
Damping parameters	β	0.00075		
	α	0		

Table 5 Material properties

Property	Concrete lining	Soil layers (1) Silty clay	(2) Sand to silty sand	(3) Sand
Modulus of elasticity, E (MPa)	20000	80	180	150
Poisson's ratio, μ	0.15	0.333	0.263	0.284
Friction angle ϕ^o	-	30^o	40^o	37^o
Cohesion, c (MPa)	-	0.2	0.15	0
Density , γ (kg/m^3)	2400	1950	1970	2000

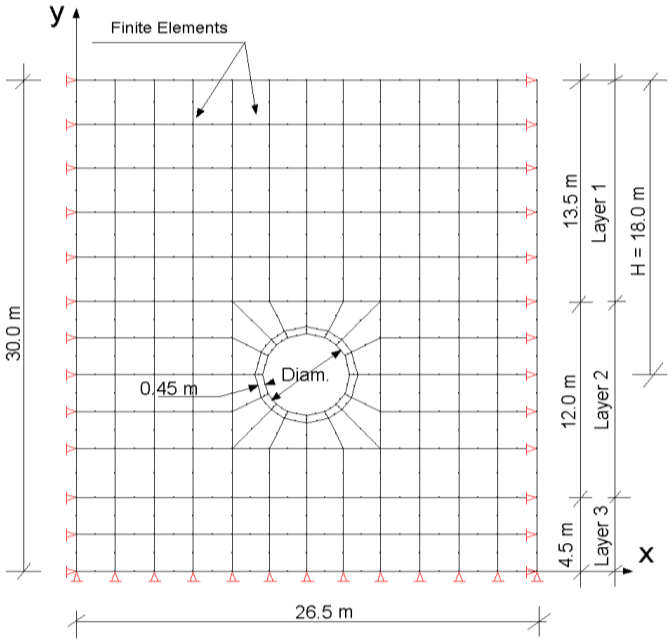

Fig. 4 Case 1 - Finite element mesh with traditional boundaries

Modeling and Boundary Conditions:

Case 1:

A finite element mesh with traditional boundaries (Fig. 4) is adopted to model the Baghdad metro line section. Isoparametric quadrilateral eight-nodded elements are used to model the concrete tunnel and the surrounding soil. The boundary side nodes are restrained laterally (only vertical displacements are possible), while the lower end nodes of the entire boundary mesh are restrained vertically (only horizontal displacements are possible).

Case 2:

The 5-node mapped infinite elements presented by Selvadurai and Karpurapu (1988) extends to infinity to the right with the other two mapped infinite elements (when infinite direction extends to the left and down), derived in this study, are added to the mesh of case 1 as shown in Fig. 5.

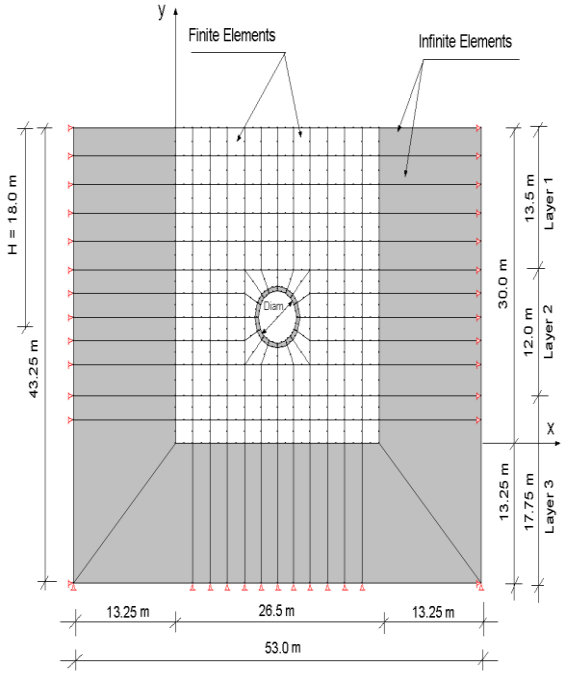

Fig. 5 Case 2 - The finite element mesh with infinite boundary elements

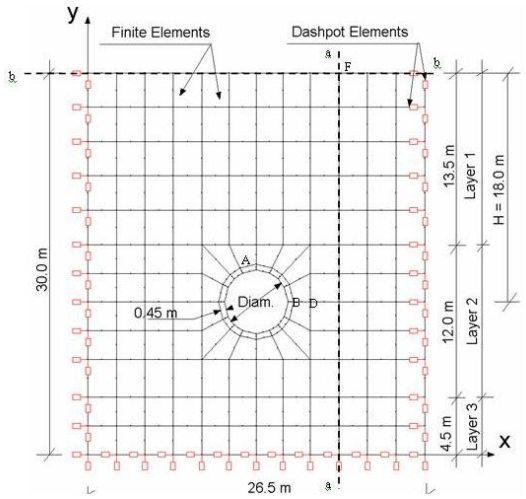

Fig. 6 Case 3 – Finite element mesh with viscous boundaries

Case 3:

A finite element mesh (as in case 1) with dashpot elements is considered to model the viscous boundaries as shown in Fig. 6.

Table 4 summarizes the general information about the finite, infinite and dashpot elements meshes for cases 1, 2 and 3. The material properties for the problem are shown in table 5.

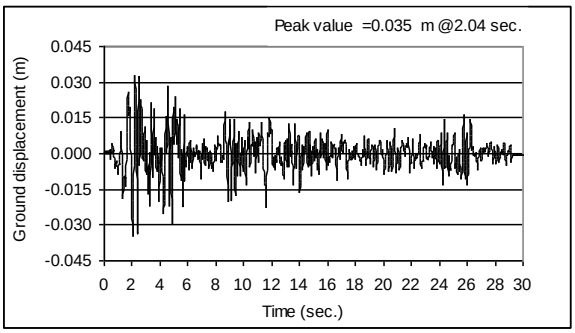

Fig. 7 The ground motion displacement time-history of El-Centro earthquake

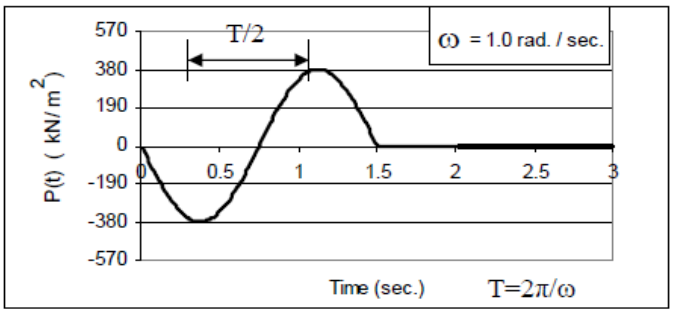

(a)

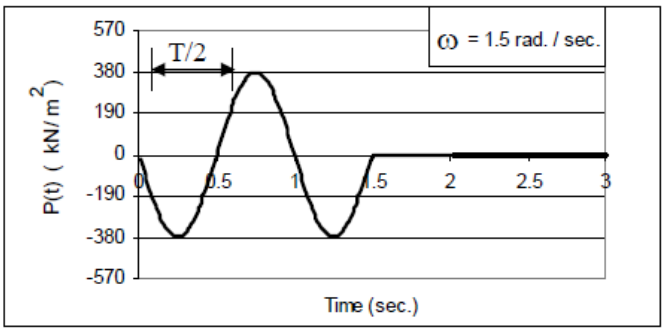

(b)

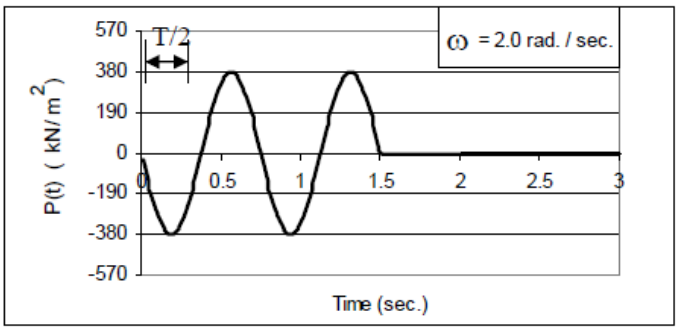

(c)

Fig. 8 Pressure load - time history for the three values of ω.

Loading:

Tunnels may be subjected to different types of dynamic loads such as earthquakes, impact loads resulting from traffic accidents if they serve as metro lines or traffic tunnels, external blast loads coming from direct or indirect hits and the internal blast loads resulting from the explosions of demolitions charges caused by sabotage works. In this study, two types of loads are considered:

1. Time-History Displacement:

The earthquake load is applied as base displacement motion. The earthquake record of El-Centro in California, which hit on 18th May 1940 has been used. It is characterized by a s magnitude equal to 6.7 on Richter scale and a peak acceleration of 0.35g. This earthquake was scaled to get three different values of peak accelerations: 0.045, 0.065 and 0.13g, which were given transformed to peak displacements Ao: 0.035, 0.05 and 0.1 m by means of the fast Fourier transform. The ground motion displacement time-history of El-Centro earthquake is shown in Fig. 7.

2. Surface Pressure Load

A sinusoidal pressure load P(t) acting at the free surface above the tunnel was adopted.

It can be represented by the following equation:

$P(t) = 380 * \sin(4.18879*\omega*t)$ kN/m^2 , for $0 < t =< 1.5$ sec.

$= 0.0$ kN/m^2 , for $1.5 < t < 3.0$ sec.

where:

ω = Angular frequency (rad./sec.).

f = Cyclic frequency (Hz). $= \omega/2\pi$

T = period (sec./rad.). $= 1/f$

Three different frequencies f: 0.16, 0.24, 0.32 Hz (ω = 1.0, 1.5, 2.0 rad./sec.) were considered for the acting sinusoidal pressure load, as shown in Fig. 8.

Parametric Study:

1. Effect of Peak Displacement:

The horizontal component of El-Centro earthquake was scaled to have three different values of peak displacement to study its effect on the behavior of the tunnel and soil.

Figs. 9 and 10 show the deflected shape of axes a-a and b-b (shown in Fig. 6) respectively at time when the peak displacement occurs along them for both cases (1 and 3), at three different values of peak displacement (Ao = 0.035m, 0.05m and 0.1m).

It can be noticed that the horizontal displacement along axis a-a increases when modeling infinite boundaries in case 3, this increase becomes larger near the ground surface about (7.0) times the value of case 1 at equal times. On the other hand, the peak value of vertical displacement decreases along axis b-b to about 0.2 the value of case 1 at about the same time.

Figs. 11 and 12 show the time history of horizontal displacement at node B (shown in Fig. 6), for both cases 1 and 3 respectively for the three different values of (Ao).

It can be concluded from these figure that the horizontal displacement on the tunnel's boundary decays significantly when using viscous boundaries (case 3) for all the considered peak displacements. This trend may be attributed to the absorption of the reflected waves made by using viscous boundaries which is faster than do the infinite elements. Figs. 15 to 20 show the normal stresses σ_x and σ_y time- history, and the shear stress τ_{xy} at node B (shown in Fig. 6) for the three different values of the peak horizontal displacement Ao for both cases 1 and 3.

A summary of the comparison between the peak values of displacements and stresses predicted at the selected locations are listed in Table 6.

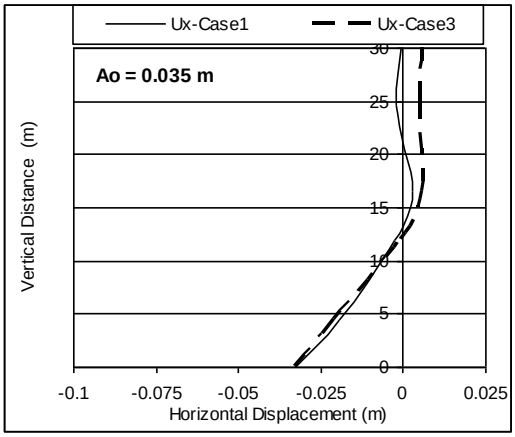

a

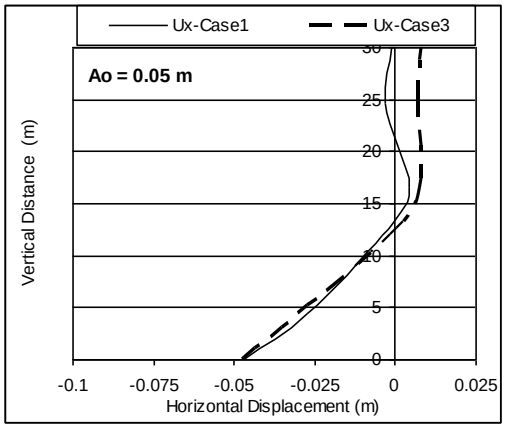

b

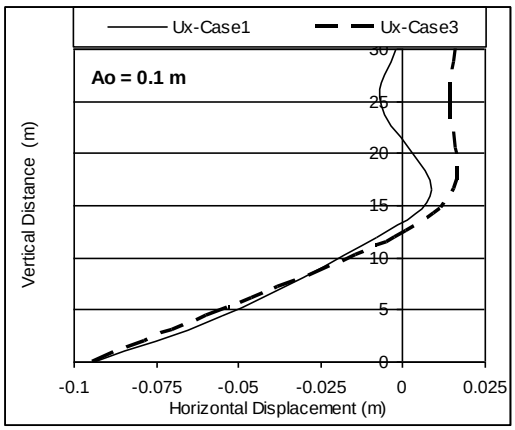

c

Fig. 9 Deflected shape of axis a-a at time of peak value of horizontal displacement for three different values of (Ao) – cases (1 and 3)

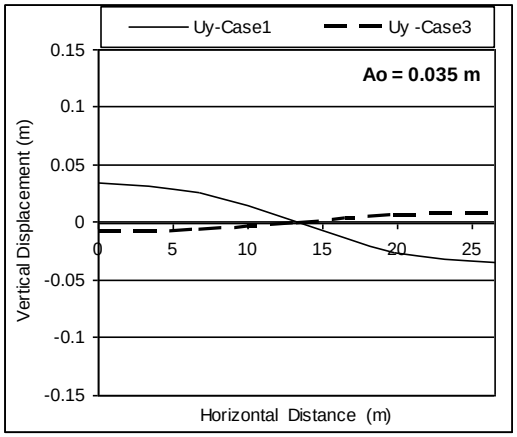

a

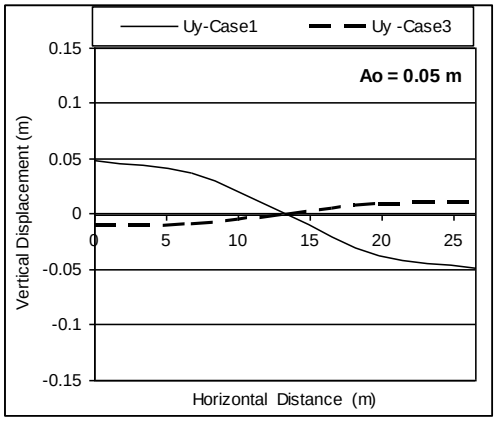

b

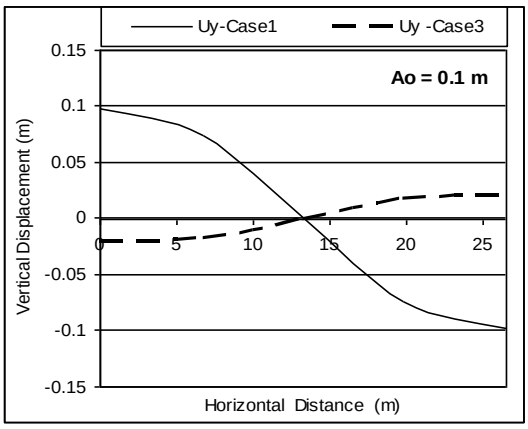

c

Fig. 10 Deflected shape of axis b-b at time of peak value of vertical displacement for three different values of (Ao) – cases (1 and 3)

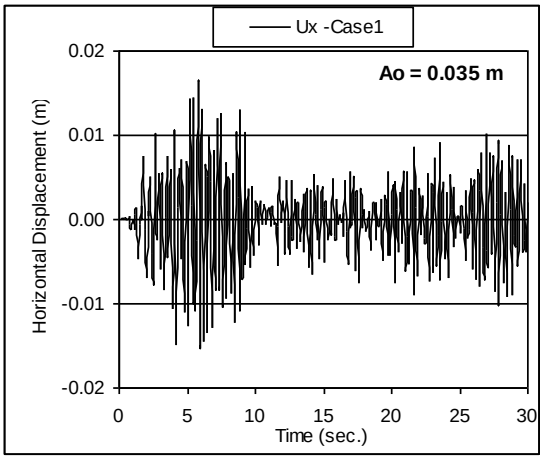

a

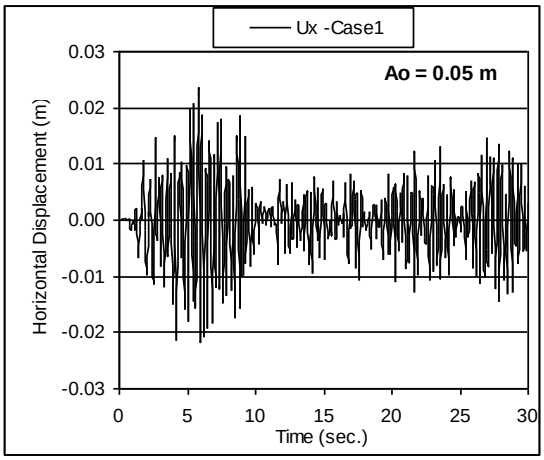

b

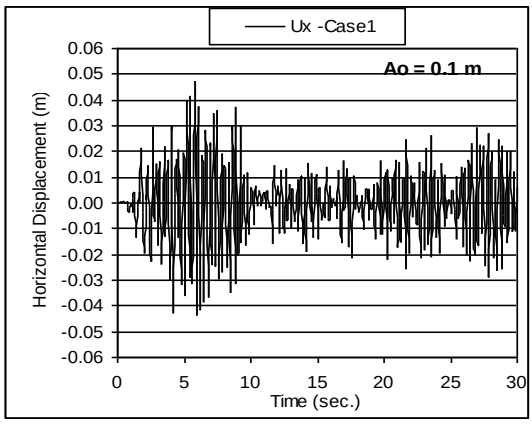

c

Fig. 11 Horizontal displacement - time history at node B for three different values of (Ao) - case (1)

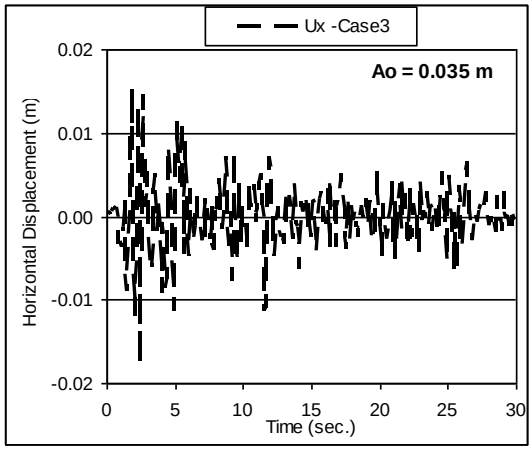

a

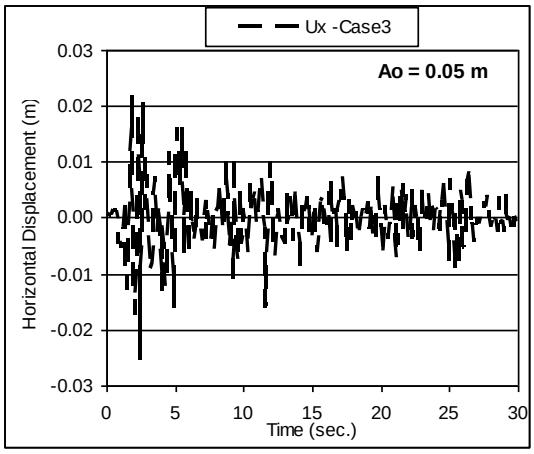

b

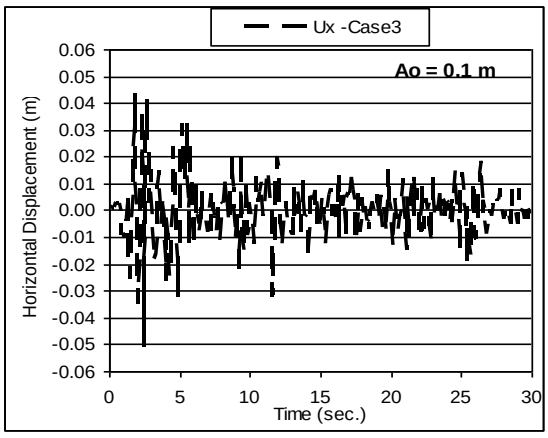

c

Fig. 12 Horizontal displacement - time history at node B for three different values of (Ao) - case (3)

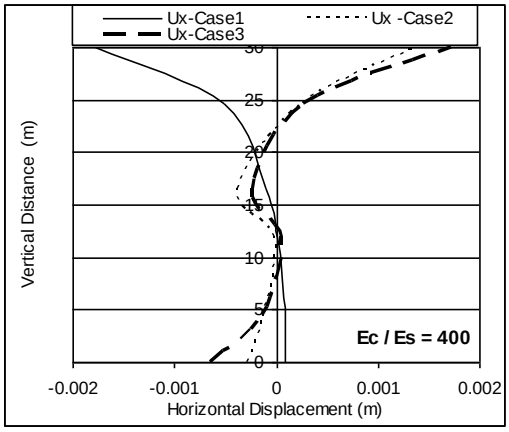

a

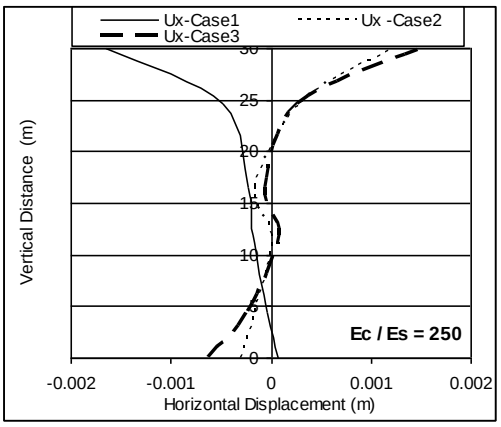

b

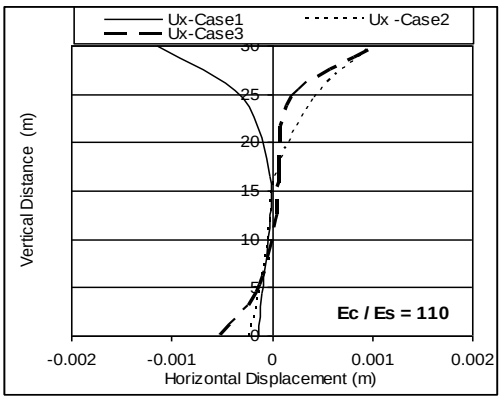

c

Fig. 13 Deflected shape of a-a axis at time of peak value of horizontal displacement for three different values of (Ec/Es) - cases (1, 2 and 3)

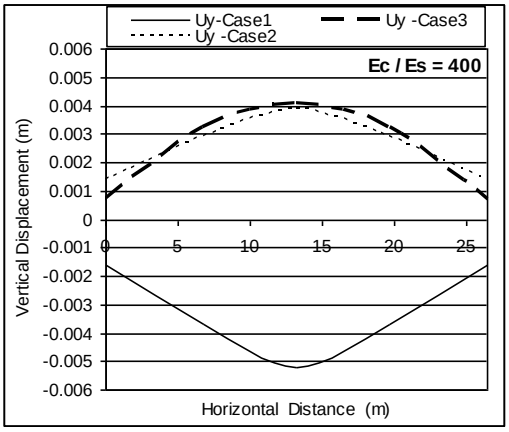

a

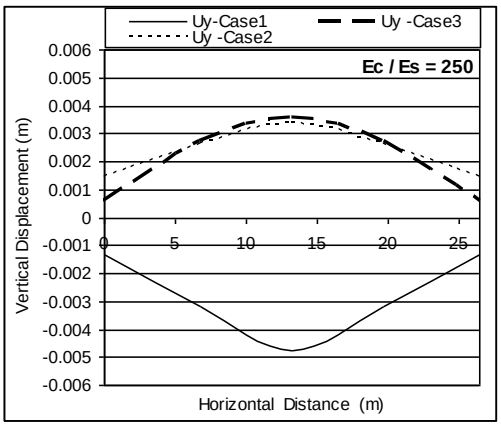

b

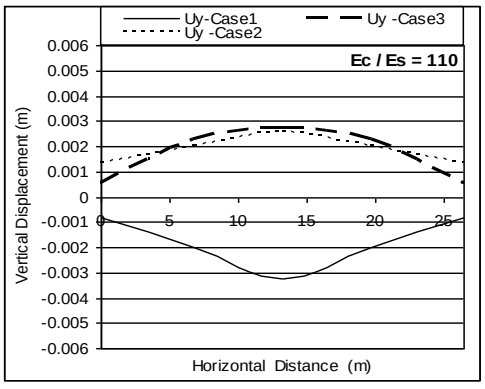

c

Fig. 14 Deflected shape of b-b axis at time of peak value of vertical displacement for three different values of (Ec/Es) - cases (1, 2 and 3)

Table 6 Comparison of results.
(a) Comparison between case 3 and case 1 for peak values of displacements and their times for
(b) axes a-a , b-b and nodes B and F at three different values of the parameter (Ao)

			Case(3)/Case(1)	
Location	Displacement	Ao (m)	Displ. ratio	Time ratio
axis a-a	Ux	0.035	1.00	1.00
		0.05	1.00	1.00
		0.1	1.00	1.00
axis b-b	Uy	0.035	-0.21	0.97
		0.05	0.21	0.97
		0.1	0.21	0.97
Node B	Ux	0.035	-1.10	0.43
		0.05	-1.10	0.43
		0.1	-1.10	0.43
Node F	Ux	0.035	-0.54	0.73
		0.05	-0.54	0.73
		0.1	-0.54	0.73

(b) : Comparison between case 3 and case 1 peak values of normal stresses σ_x , σ_y and shear stress τ_{xy} at node B for three different values of parameter (Ao)

		Case(3)/Case(1)	
Stresses	Ao (m)	Stress ratio	Time ratio
σ_x	0.035	0.83	1.87
	0.05	0.83	1.87
	0.1	0.84	1.87
σ_y	0.035	-0.92	1.84
	0.05	-0.92	1.84
	0.1	-0.92	1.84
τ_{xy}	0.035	0.85	0.09
	0.05	0.85	0.09
	0.1	0.85	0.09

Effect of the Modular Ratio (Ec/Es):

By applying the impulse load IL(t), (shown in Fig. 10) at node G (shown in Fig. 6), the effect of the ratio of the modulus of elasticity of the concrete lining to that of the soil surrounding the tunnel (soil layer type 2) is studied.

Figs. 13 and 14 show the deflected shape of a-a and b-b axes respectively at time when peak

Table 7: Effect of the modular ratio on stresses and displacements.
(a): A comparison between cases 2, 3 and case 1 peak values of displacements and their times for a-a , b-b axes and nodes A and F at three different values of parameter (Ec/Es)

			Case(2)/Case(1)		Case(3)/Case(1)	
Location	Displacement	Ec/Es	Displ. ratio	Time ratio	Displ. ratio	Time ratio
a-a axis	Ux	400	0.80	0.94	-0.98	0.71
		250	0.82	0.94	-0.92	0.70
		110	0.88	4.56	-0.99	0.73
b-b axis	Uy	400	0.94	0.94	-0.79	0.36
		250	0.93	1.00	-0.75	0.36
		110	0.93	0.94	-0.85	0.39
Node A	Uy	400	0.97	0.89	1.00	1.00
		250	0.98	0.89	1.00	1.00
		110	0.98	1.00	1.00	1.00
Node F	Ux	400	0.80	0.94	-0.98	0.71
		250	0.82	0.94	-0.92	0.70
		110	0.88	4.56	-0.99	0.73

(b): A comparison between case 3 and case 1 peak values of normal stresses σ_x , σ_y and shear stress τ_{xy} for nodes A, B and D at three different values of parameter (Ec/Es)

			Case(3)/Case(1)	
Node	Stresses	Ec/Es	Stress ratio	Time ratio
A	σ_x	400	1.00	1.00
		250	1.00	1.00
		110	1.00	1.00
D	σ_x	400	1.00	1.00
		250	1.00	1.00
		110	0.99	1.00
B	σ_y	400	1.00	1.00
		250	1.00	1.00
		110	1.01	1.00
D	σ_y	400	-0.50	0.41
		250	0.45	1.00
		110	0.44	0.35
B	τ_{xy}	400	1.00	1.00
		250	1.00	1.00
		110	1.00	1.00
D	τ_{xy}	400	1.00	1.00
		250	1.00	1.00
		110	1.00	1.00

displacement occurs along them, for three different values of Ec/Es, (Ec/Es = 400, 250, 110), (Es = 50×10^3, 80×10^3, 180×10^3 kN/m^2).

It is noticed from these figure that considering infinite boundaries reverse the direction of the deflected shapes of a-a and b-b axes for the three values of Ec/Es ratio.

On the other hand, it is concluded that using viscous boundaries has a considerable effect on the peak value of the vertical displacement along b-b axis which decreases about 25% from the value of case (1), and it reaches the peak value faster 2.8 times than in case (1).

Modeling of infinite elements in problems of tunnels in clayey ground causes the settlement trough which takes the shape of the normal probability distribution to be larger.

Fig. 15 shows the time-history of vertical displacement at node A (shown in Fig. 6), for the three different values of Ec/Es ratio at the three cases 1, 2 and 3.

Fig. 16 shows the time-history of horizontal displacement at node F (shown in Fig. 6), for the same condition.

It can be observed that there is a little effect of the presence of infinite boundaries on the peak values of the displacements at node A, but it has (especially in case (3)) a considerable effect on the absorbing the waves rapidly than in case (1).

Figs. 17 and 18 present the time-history of the normal stress σ_x at nodes A and D respectively under the three different values of Ec/Es and for both cases 1 and 3. Figs. 19 to 22 present the time-history of the normal stress σ_y and shear stress τ_{xy} at nodes B and D under the same above conditions.

A summary of comparison between the peak values of displacements and stresses of the Figs. 13 to 22 are listed in Table 7.

Effect of the Tunnel's Diameter:

By applying the impulse load IL (t) (shown in Fig. 8) at node G (shown in Fig. 6), the effect of three different values of the ratio H/Diam is studied where (H) is the tunnel's depth while (Diam) is the inner diameter of the tunnel.

Figs. 23 and 24 show the deflected shape of a-a and b-b axes respectively at the time when the peak values of displacements occur along them for three different values of H/Diam ratio (H/Diam = 4, 3.6 and 3.27), (Diam = 4.5, 5.0 and 5.5 m) for cases 1, 2 and 3. It is noticed that considering infinite boundaries changes the direction of the deflected shapes of a-a and b-b axes for the three values of H/Diam ratio.

Figs. 25 and 26 show the time history of vertical displacement at node A and horizontal displacement at node B (shown in Fig. 6) respectively for the three different values of H/Diam ratio for the cases 1, 2 and 3. It can be observed that there is a little effect of the presence of infinite boundaries on the peak values of the displacements, but case (3) where dashpots are used has a considerable effect on absorbing the waves rapidly than in case (1).

Figs. 27 and 28 present the time-history of the normal stress σ_x at nodes A and B respectively under different values of H/Diam and for both cases 1 and 3. Figs. 29 to 32 present the time-history of the normal stress σ_y and shear stress τ_{xy} at nodes B and D under the same condition.

A summary of comparison between the peak values of displacements and stresses of the Figs. 23 to 32 are listed in Table 8.

Table 8: Effect of tunnel's diameter

(a): A comparison between case 2, 3 and case 1 peak values of displacements and their times fora-a , b-b axes and nodes A and F at three different values of parameter (H/Diam)

			Case(2)/Case(1)		Case(3)/Case(1)	
Location	Displacement	H/Diam	Displ. ratio	Time ratio	Displ. ratio	Time ratio
a-a axis	Ux	4	0.92	4.56	-1.00	0.73
		3.6	0.88	4.56	-0.99	0.73
		3.27	0.84	4.56	-0.96	0.73
b-b axis	Uy	4	0.93	0.94	-0.85	0.39
		3.6	0.93	0.94	-0.85	0.39
		3.27	0.93	1.00	-0.86	0.36
Node A	Uy	4	0.98	0.89	1.01	1.13
		3.6	0.98	1.00	1.00	1.00
		3.27	0.97	1.00	1.01	1.00
Node F	Ux	4	0.92	4.56	-1.00	0.73
		3.6	0.88	4.56	-0.99	0.73
		3.27	0.84	4.56	-0.96	0.73

(b) : A comparison between case 3 and case 1 peak values of normal stresses (σ_x , σ_y) and shear stress (τ_{xy}) for nodes A, B and D at three different values of parameter (H/Diam)

			Case(3)/Case(1)	
Node	Stresses	H/Diam	Stress ratio	Time ratio
A	σ_x	4	1.00	1.00
		3.6	1.00	1.00
		3.27	1.00	1.00
D	σ_x	4	0.99	1.00
		3.6	0.99	1.00
		3.27	0.99	1.00
B	σ_y	4	1.00	1.17
		3.6	1.01	1.00
		3.27	1.01	1.00
D	σ_y	4	-0.44	1.61
		3.6	0.44	0.35
		3.27	0.44	0.35
B	τ_{xy}	4	1.00	1.00
		3.6	1.00	1.00
		3.27	1.00	1.00
D	τ_{xy}	4	1.00	1.00
		3.6	1.00	1.00
		3.27	1.00	1.00

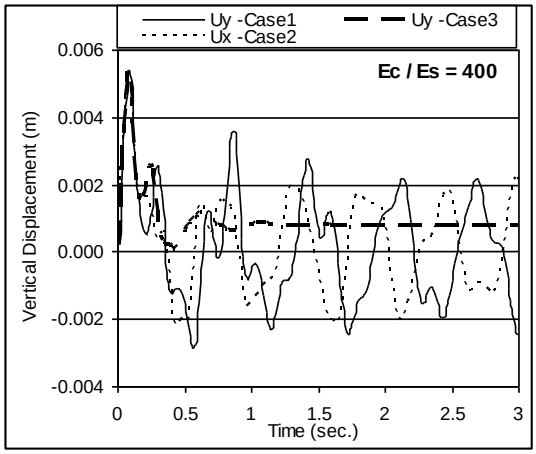

a

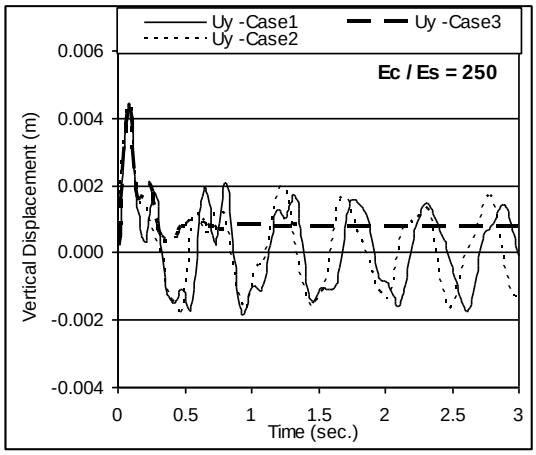

b

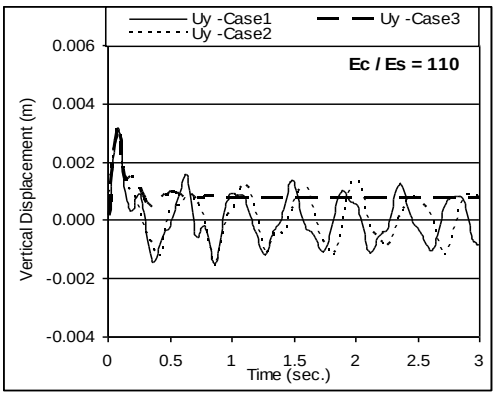

c

Fig. 15 Vertical displacement - time history at node (A) for three different values of (Ec/Es) - cases (1, 2 and 3)

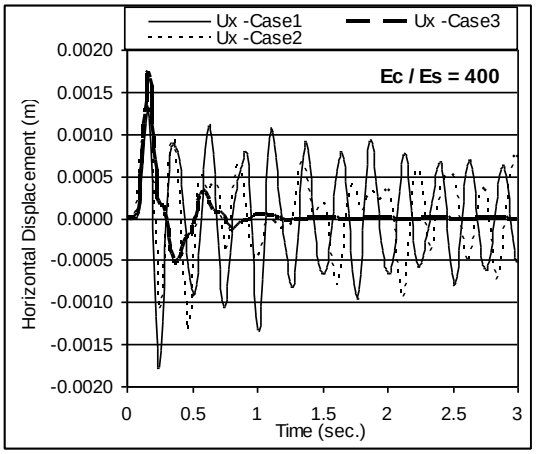

a

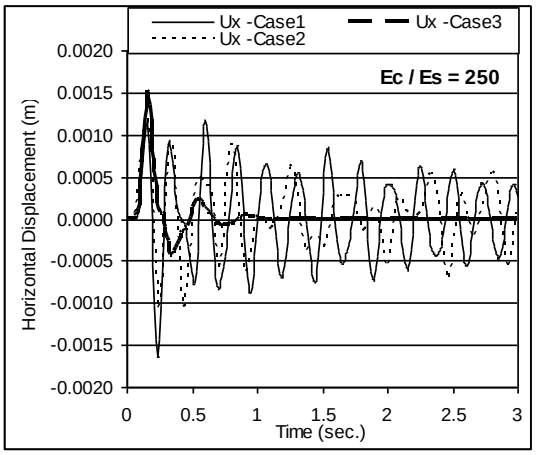

b

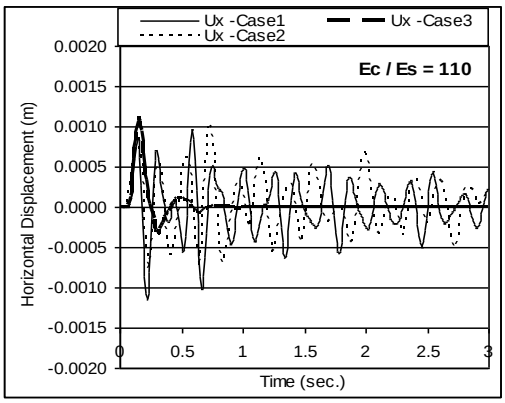

c

Fig. 16 Horizontal displacement - time history at node (F) for three different values of (Ec/Es) - cases (1, 2 and 3)

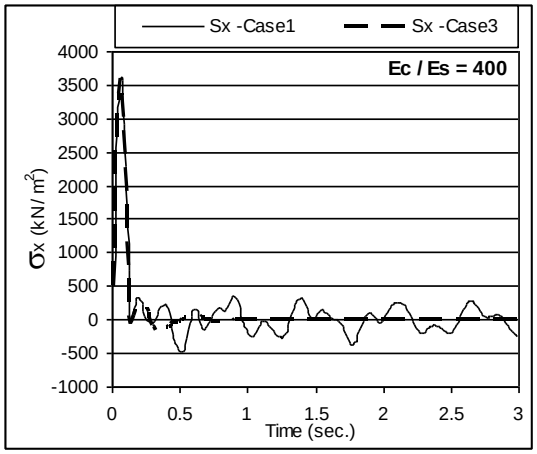

a

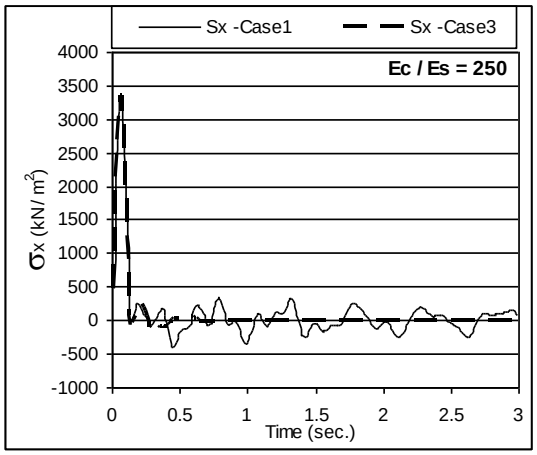

b

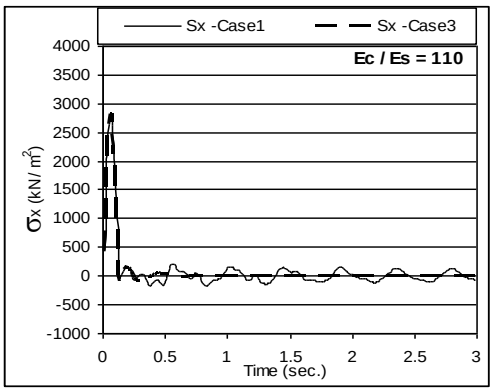

c

Fig. 17 Normal stress (σx) - time history at node (A) for three different values of (Ec/Es) - cases (1 and 3)

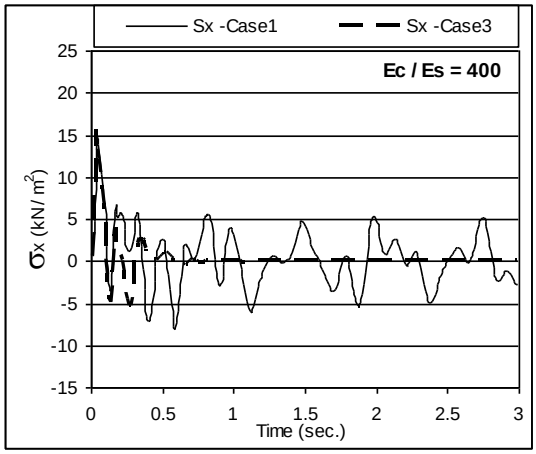

a

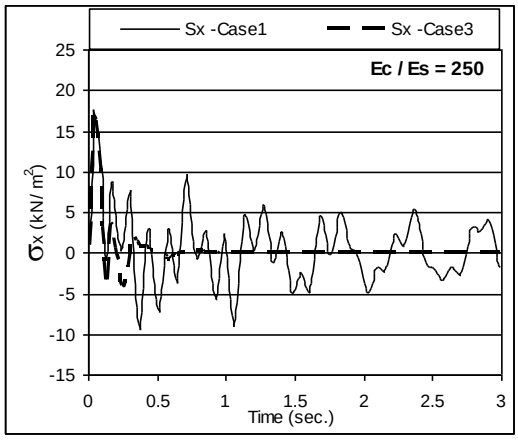

b

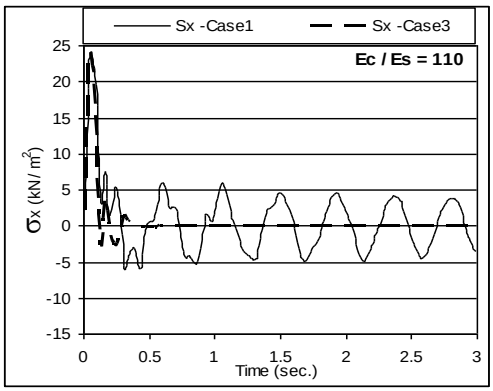

c

Fig. 18 Normal stress (σx) - time history at node (D) for three different values of (Ec/Es) - cases (1 and 3)

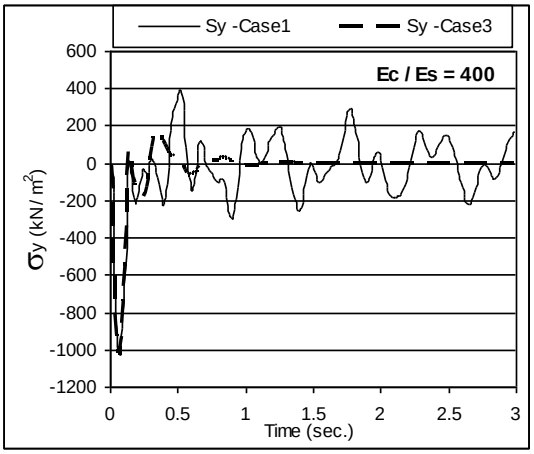

a

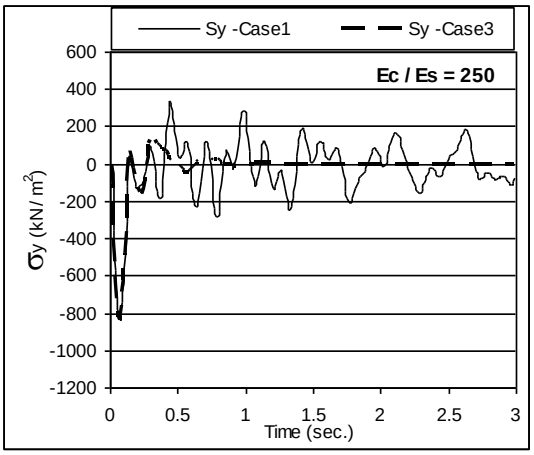

b

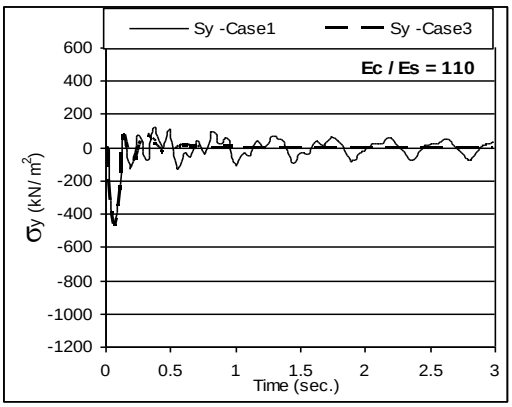

c

Fig. 19 Normal stress (σy) - time history at node (B) for three different values of (Ec/Es) - cases (1 and 3)

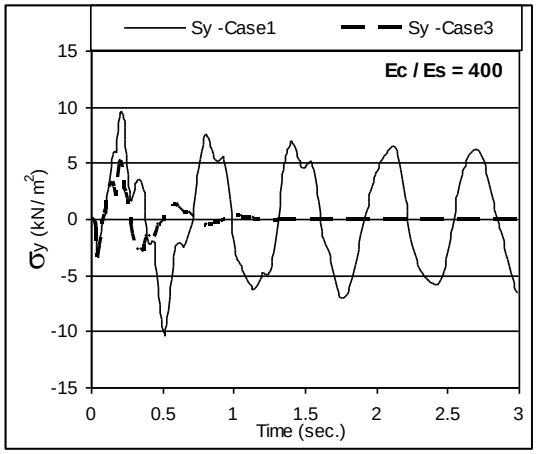

a

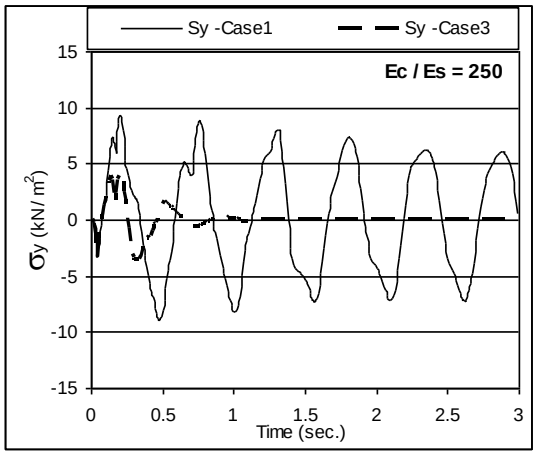

b

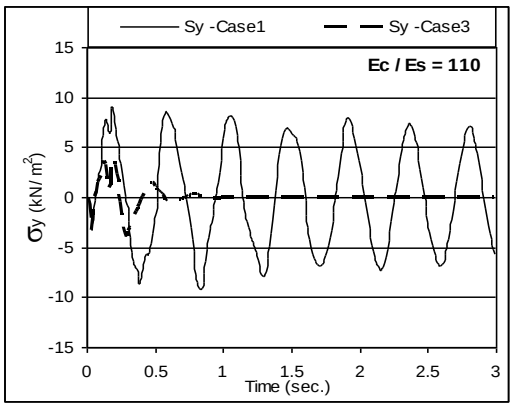

c

Fig. 20 Normal stress (σy) - time history at node (D) for three different values of (Ec/Es) - cases (1 and 3)

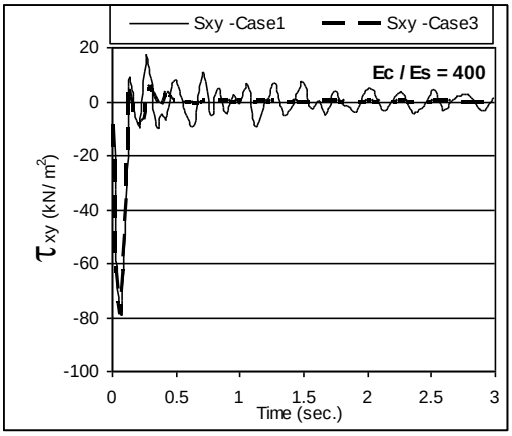

a

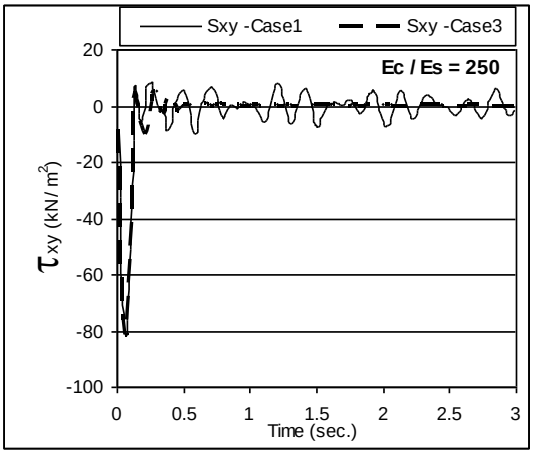

b

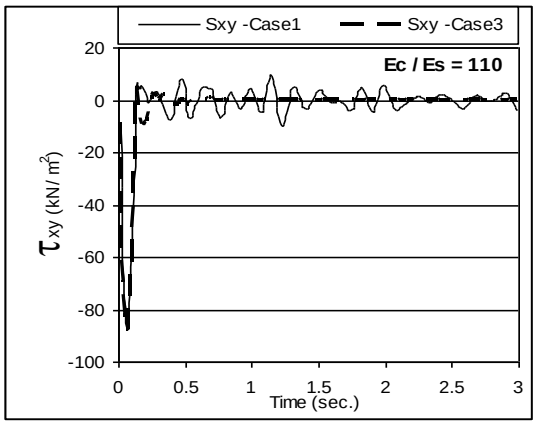

c

Fig. 21 Shear stress (τxy) - time history at node (B) for three different values of (Ec/Es) - cases (1 and 3)

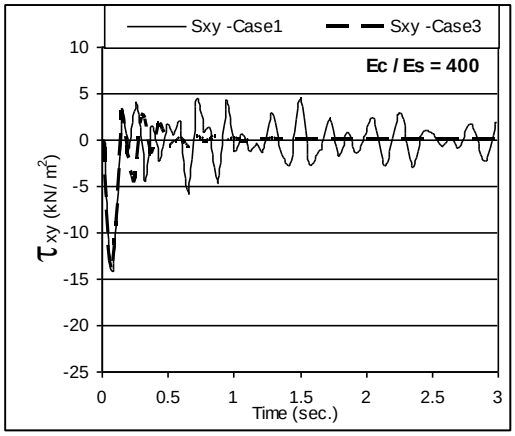

a

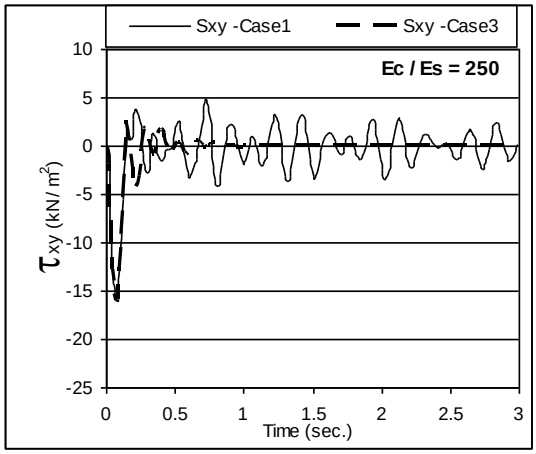

b

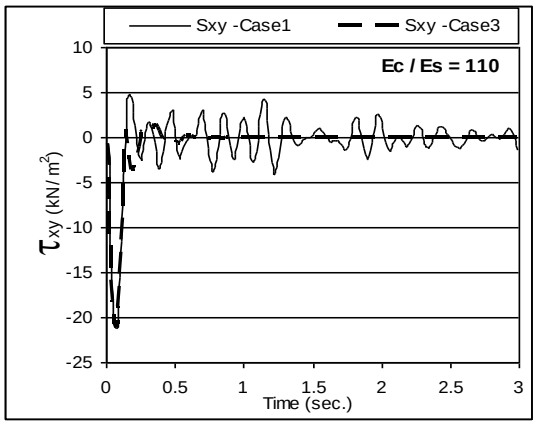

c

Fig. 22 Shear stress (τxy) - time history at node (D) for three different values of (Ec/Es) - cases (1 and 3)

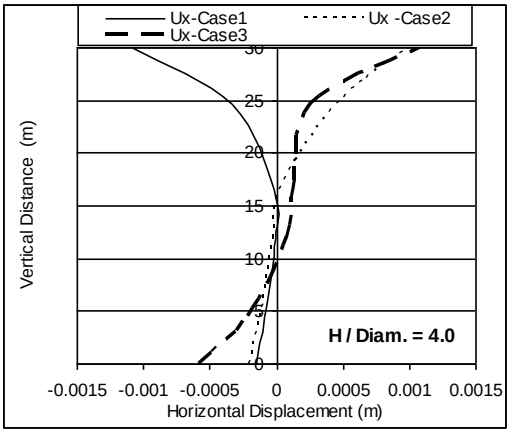

a

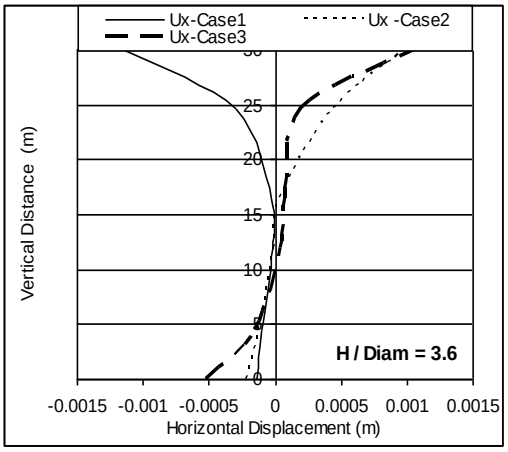

b

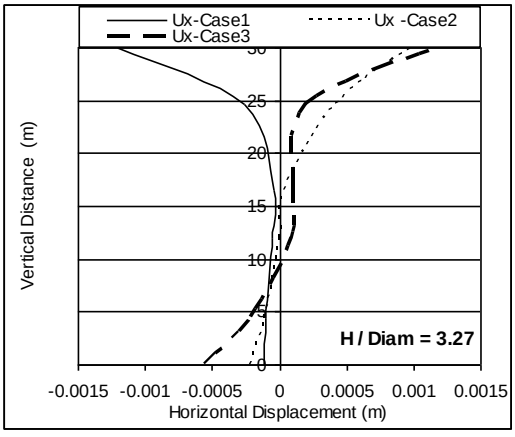

c

Fig. 23 Deflected shape of a-a axis at time of peak value of horizontal displacement for three different values of (H/Diam.) - cases (1, 2 and 3)

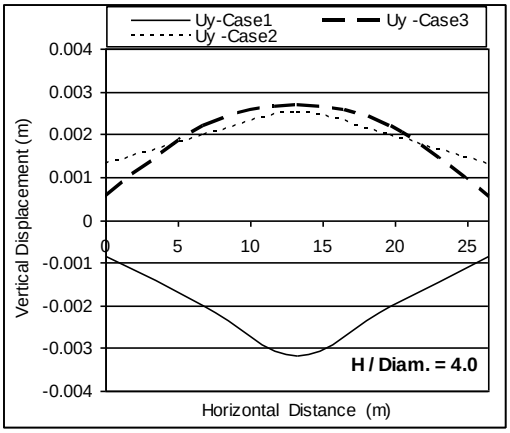

a

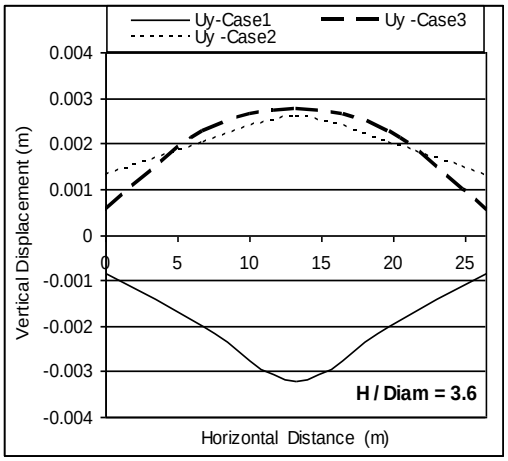

b

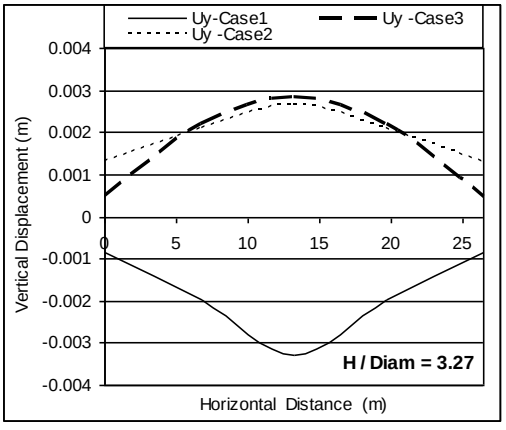

c

Fig. 24 Deflected shape of b-b axis at time of peak value of vertical displacement for three different values of (H/Diam.) - cases (1, 2 and 3)

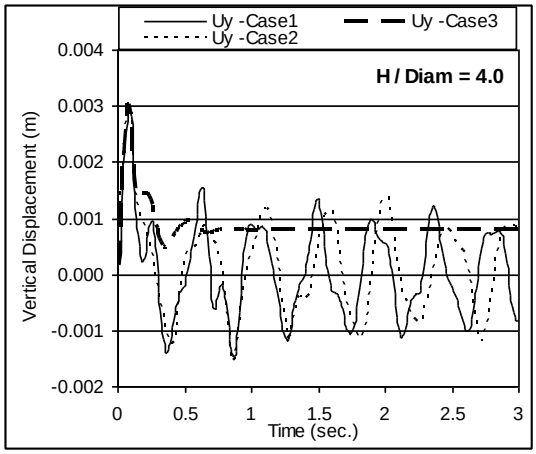

a

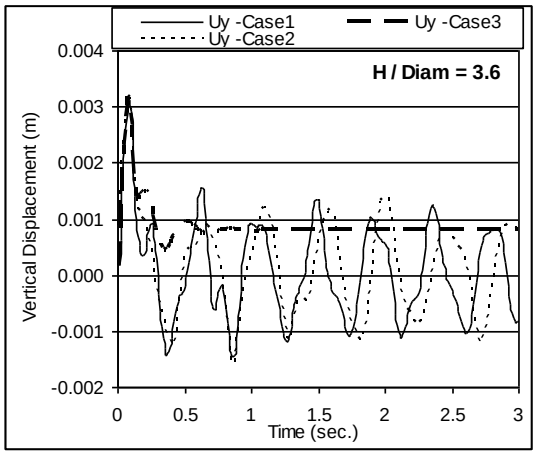

b

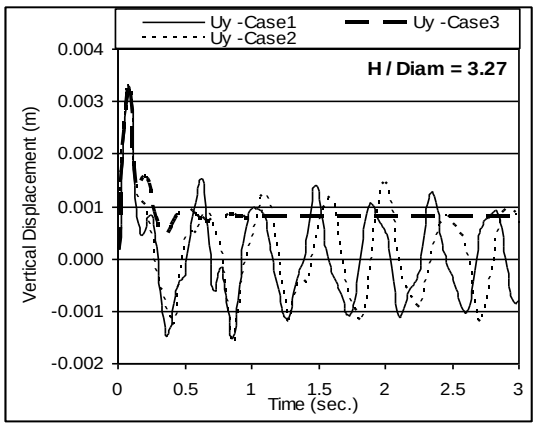

c

Fig. 25 Vertical displacement - time history at node (A) for three different values of (H/Diam.) - cases (1, 2 and 3)

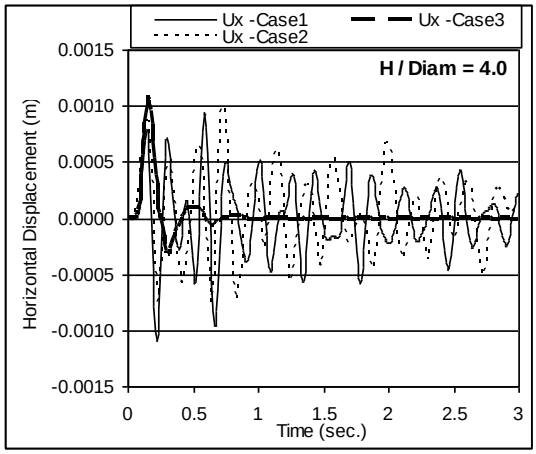

a

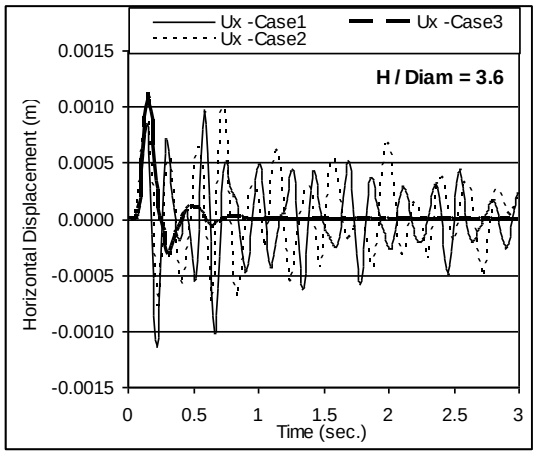

b

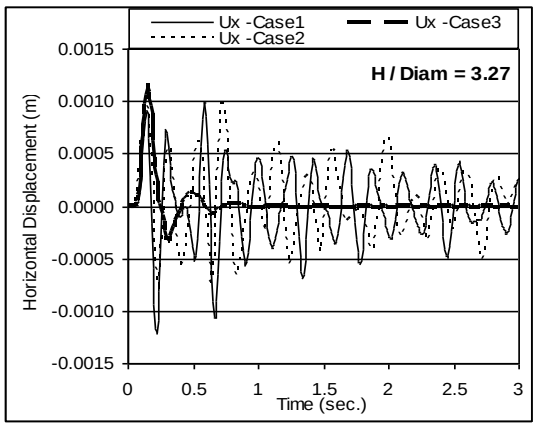

c

Fig. 26 Horizontal displacement - time history at node (F) for three different values of (H/Diam.) - cases (1, 2 and 3)

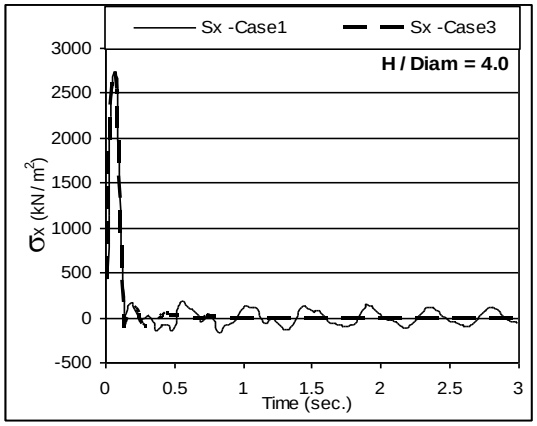

a

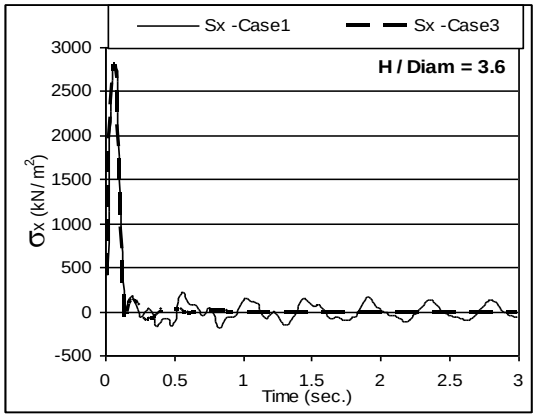

b

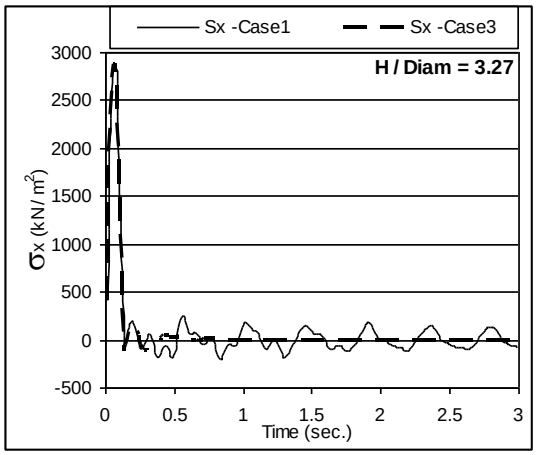

c

Fig. 27 Normal stress (σx) - time history at node (A) for three different values of (H/Diam.) - cases (1 and 3)

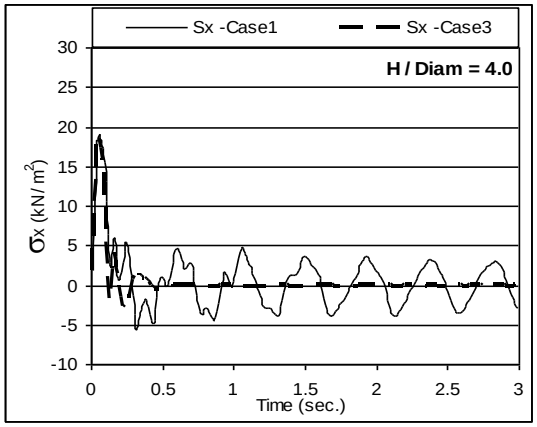

a

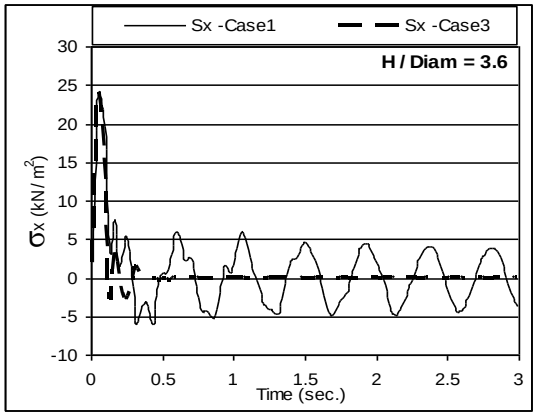

b

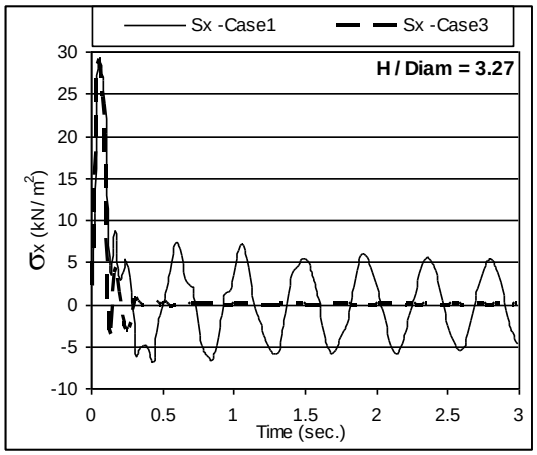

c

Fig. 28 Normal stress (σx) - time history at node (D) for three different values of (H/Diam.) - cases (1 and 3)

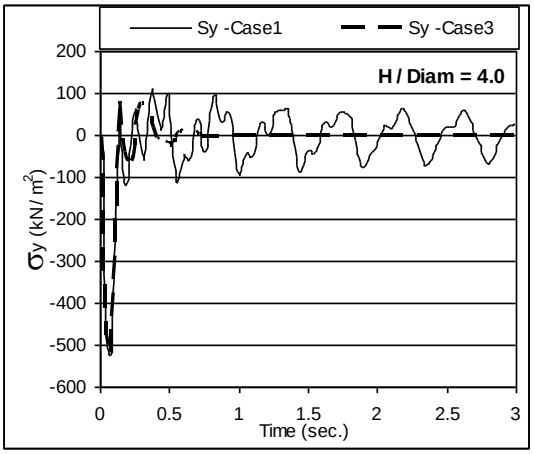

a

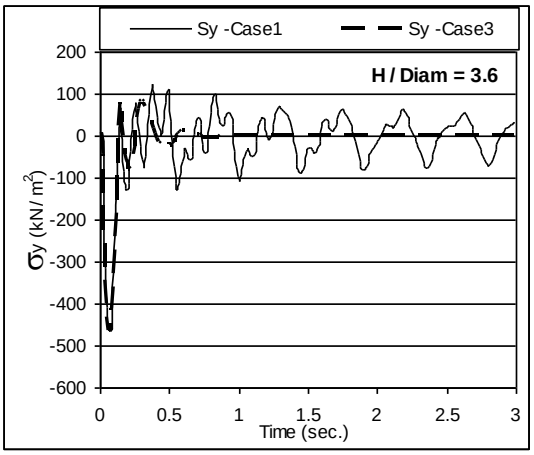

b

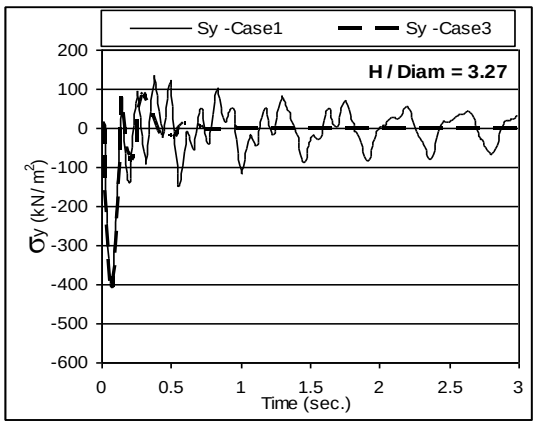

c

Fig. 29 Normal stress (σy) - time history at node (B) for three different values of (H/Diam.) - cases (1 and 3)

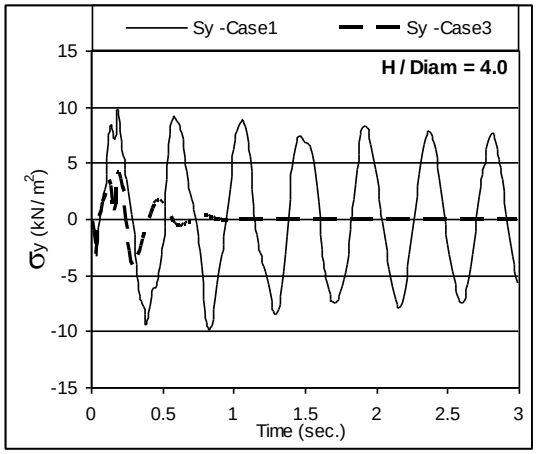

a

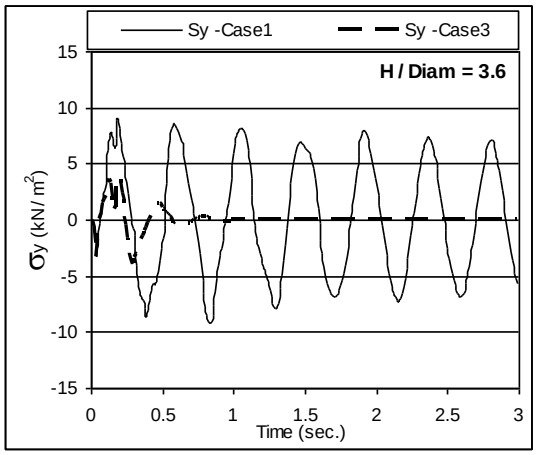

b

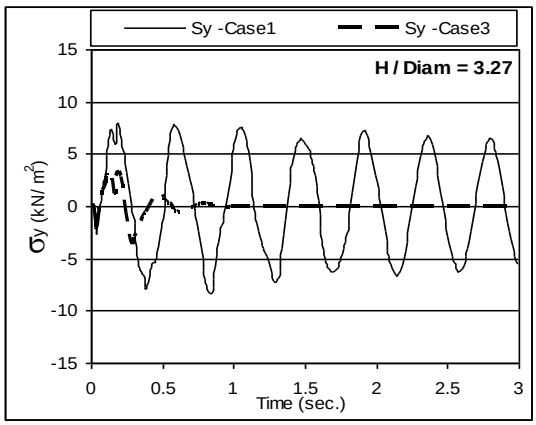

c

Fig. 30 Normal stress (σy) - time history at node (D) for three different values of (H/Diam.) - cases (1 and 3)

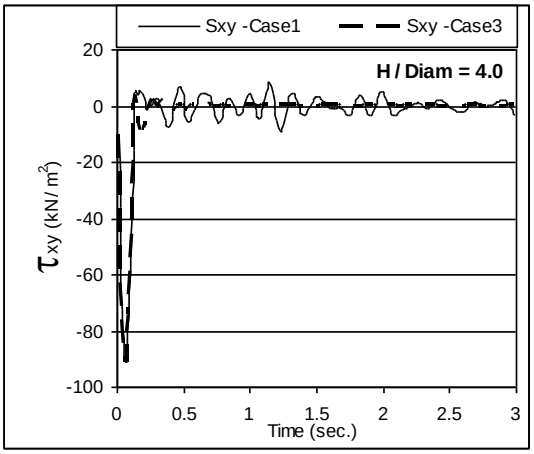

a

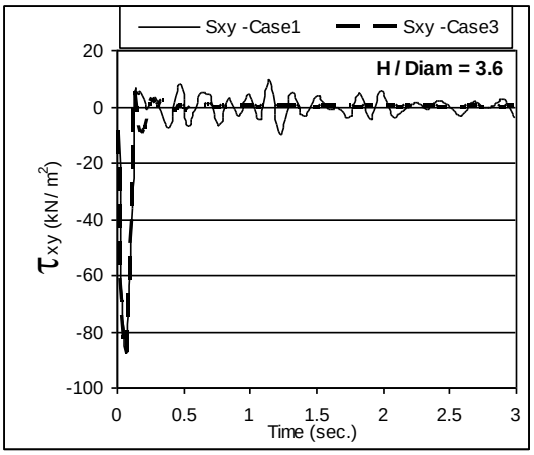

b

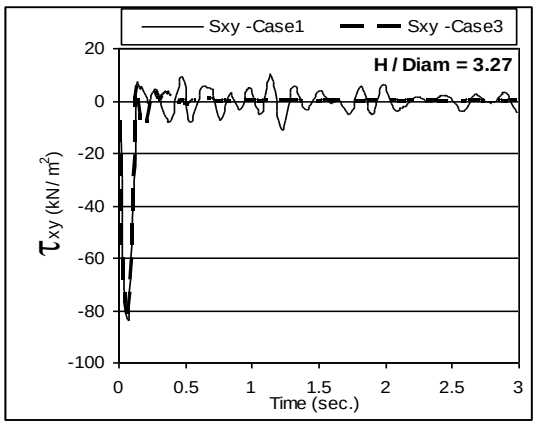

c

Fig. 31 Shear stress (τxy) - time history at node (B) for three different values of (H/Diam.) - cases (1 and 3)

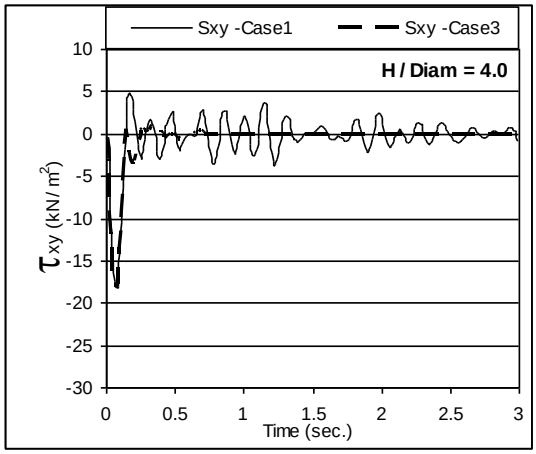

a

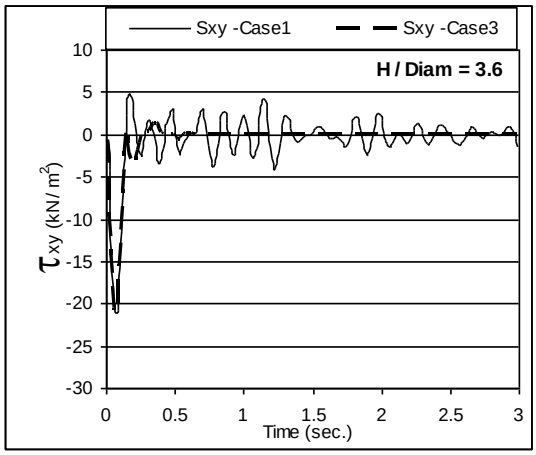

b

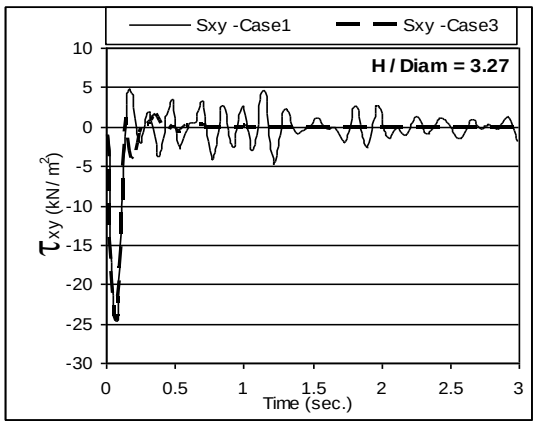

c

Fig. 32 Shear stress (τxy) - time history at node (D) for three different values of (H/Diam.) - cases (1 and 3)

7. Conclusions

A dynamic finite-element analysis is carried out for a soil-structure interaction problem considering transmitting boundaries. Two types of boundaries are considered in addition to the traditional boundaries: viscous boundaries and mapped infinite elements. The following conclusions are drawn:

1) The transmitting boundary absorbs most of the incident energy. The distinct reflections observed for the "fixed boundaries" disappear by using "transmitted boundaries". This is true for both cases of using viscous boundaries or mapped infinite elements.

2) The type and location of the dynamic load represent two controlling factors in deciding the importance of using infinite boundaries. It was found that the results present significant differences when earthquake is applied as a base motion or a pressure load is applied at the surface ground.

3) The horizontal displacement on the free surface increases significantly when modeling infinite boundaries for all values of the earthquake peak displacement. It increases about 7.0 times the value obtained by using finite elements only.

4) The peak value of the vertical displacement at nodes A, B, E and F (located at the tunnel's crown and side walls, and at the surface above the tunnel and at the surface 6.5 m away from tunnel's centre respectively) increases with the frequency of the surface pressure load for both cases 1 and 2 (traditional boundaries and mapped infinite elements respectively) while it decreases for case 3 (viscous boundaries).

5) The modular ratio Ec/Es (modulus of elasticity of the concrete lining to that of the surrounding soil) has a considerable effect on the peak value of the horizontal displacement at node B (on the side wall of the tunnel lining) increase about (17.5) times, for the three cases (1, 2, and 3).

6) Considering infinite boundaries changes the direction of the deflected shape of a-a and b-b axes (located at the surface and at a distance about 6.5 m from the tunnel's center respectively) for the three values of H/Diam ratio (H: the tunnel depth, Diam: the inner diameter of the tunnel).

7) There is a little effect of the presence of infinite boundaries on the peak values of the displacements but case(3) where dashpots are used has a considerable effect on absorbing the waves rapidly than in case (1).

Reference

Abdel-Fattah, T.T., Hodhod, H.A. and Akl, A.Y. (2000), "A novel formulation of infinite elements for static analysis", *Comput. Struct.*, 77, 371-379.

Beer, G. and Meek, J.L. (1981), "Infinite domain elements", , **17**, 43-52.

Bettess, P. (1977), "Infinite Elements", *Int. J. Numer. Method Eng.*, **11**.

Bettess, P. (1992), "Infinite Elements", first edition, Penshaw Press.

Engquist, B. and Majda, A. (1979), "Radiation boundary conditions for acoustic and elastic wave calculations", *Communi. Pure and Appl. Math.*, **32**, 313-357.

Feltrin, G. (1997), "Absorbing Boundaries for Time-Domain Analysis of Dam-Reservoir-Foundation Systems", Swiss Federal Institute of Technology Zurich, Nov.

Karpurapu, G.R. (1988), "Composite Infinite Element Analysis of Unbounded Two-Phase Media", Computational Mechanics Publications / Adv. Eng. Software, **10**(4).

Lysmer, J. and Kuhlemeyer, R.L. (1969), "Finite dynamic model for infinite media", *J. Eng. Mech.*, ASCE,

95(EM4).
Mahmoudpour, S., Attarnejad, R. and Behnia, C. (2011), "Dynamic analysis of partially embedded Structures Considering Soil-Structure Interaction in Time Domain", Mathematical Problems in Engineering, Volume 2011, Article ID 534968, 23 pages, Hindawi Publishing Corporation.
Medina, F. and Penzien, J. (1982), "Infinite elements for elastodynamics.", *Earthq. Eng. Struct. Dyn.*, **10**.
Medina, F. and Taylor, R.L. (1983), "Finite element techniques for problems of unbounded domains", *Int. J. Numer.Method Eng.*, **19**(8), 1209–1226.
Owen, D.R.J. and Hinton, E. (1980), "Finite elements in plasticity: Theory and practice", Pineridge Press Limited.
Patil, V.A. Sawant, V.A. and Deb, K. (2010), "Use of Infinite Elements in the Dynamic Analysis of Rigid Pavement Resting on Two Parameter Soil Medium", Indian Geotechnical Conference – 2010, GEOtrendz, December 16–18, 2010, IGS Mumbai Chapter & IIT Bombay, 895-898.
Ryua, J.S., Seob, C.G., Kimc, J.M. and Yund, C.B. (2010), "Seismic response analysis of soil–structure interactive system using a coupled three-dimensional FE–IE method", *Nuclear Eng. Des.*, **240**, 1949–1966.
Selvadurai, A.P.S. and Gopal, K.R. (1986), "Consolidation analysis of screw plate test", *Proceeding of the 39th Canadian Geotech. Conference*, Ottawa. 167-178.
Su, J. and Wang, Y. (2013), "Equivalent dynamic infinite element for soil-structure interaction", *Finite Elements Anal. Des.*, **63**, 1-7.
Yun, C.B., Kim, J.M. and Hyun, C.H. (1995), "Axisymmetric elastodynamic infinite elements for multi-layered half-space", *Int. J. Numer. Method Eng.*, **38**, 3723-3743.
Takewaki, I., Fujii, N. and Uetani, K. (2002), "Simplified inverse stiffness design for nonlinear soil amplification", *Eng. Struct.* , **24**(11), 1369-1381.
Zakeri, J. A. Xia, H. (2009), "Application of 2D-infinite beam elements in dynamic analysis of train-track interaction", *J. Mech. Sci. Technol.*, **23**, 1415-1421.
Zhao, C. and Valliappan, S. (1993), "An efficient wave input procedure for infinite media", *Commun. Numer. Method Eng.*, **9**, 407-415.
Zienkiewicz, O.C., Emson, C. and Bettess, P. (1983), "A novel boundary infinite element", *Int. J. Numer.Method Eng.*, **19**, 393-404.

IT